RESEARCH PAPER

Effect of Copper Dopant on Microstructural and Optical Properties of NiTiO$_3$ Ilmenite Materials Synthesized by Citrate Method

Nguyen Hoang Thoan[1], Pham Phi Hung[2], Dang Duc Dung[1], Tran Vu Diem Ngoc[3], Luong Huu Bac[1,]*

[1] School of Engineering Physics, Ha Noi University of Science and Technology,1 Dai Co Viet, Ha Noi, Viet Nam

[2] Viet Nam Metrology Institute, 8 Hoang Quoc Viet, Cau Giay, Ha Noi, Viet nam

[3] School of Engineering Materials and Technology, Ha Noi University of Science and Technology, 1 Dai Co Viet, Ha Noi, Viet Nam

ARTICLE INFO

ABSTRACT

In this work, the Ni$_{1-x}$Cu$_x$TiO$_3$ ($0 \leq x \leq 0.1$) ilmenite materials were successfully synthesized using the citrate-gel method using nickel nitrate, copper nitrate and titanium (IV) isopropoxide as Ni, Cu, Ti sources and citric acid as complexing reagent. The evolution of the microstructural properties was investigated using X-ray diffraction (XRD) and scanning electron microscopy (SEM). Powder X-ray diffraction pattern confirms the formation of the ilmenite phase for all the samples. The particle size of the prepared samples substantially increased with increase of copper dopant content. The study of phonon vibration by Raman spectroscopy identified a change in structure of NiTiO$_3$ due to Cu dopant. The optical properties with the Cu content was carried out using UV-vis absorption spectroscopy. The reduction of optical band gap from 2.31 eV to 1.99 eV was obtained for undoped NiTiO$_3$ and 10 mol.% Cu dopant in NiTiO$_3$, respectively. To evaluate the photocatalyst properties of NiTiO$_3$, the photocatalytic degradation of congo red under visible light irradiation was carried out. Our results revealed that the copper dopant into NiTiO$_3$ lattice promoted the increase of particle size, decrease of optical bandgap and enhancement of textile photodegradation.

How to cite this article

INTRODUCTION

Titanates materials with the formula MTiO$_3$, where M is a transition metal such as Fe, Co, Ni, Mn, Cu, Zn have been concerned for functional inorganic materials in many applications including solid oxide fuel cells, gas sensors, solid lubricants, pigment and photocatalyst. Among titanate materials, nickel titanate (NiTiO$_3$) is an important member of MTiO$_3$ material family, in which both Ni^{2+} and Ti^{4+} possess an octahedral on each alternating cation layer of the compound, which is occupied by either Ni^{2+} and Ti^{4+} cations solely [1]. This material has been investigated for application in many fields, such as visible-light photocatalysis [2], solid oxide fuel cells [3], gas or glucose sensor [4,5], spin electronic devices with magnetoelectric effect [6], and paint pigment [7], anode materials for lithium-ion batteries [8] due to its multifunctional ability. NiTiO$_3$ is an *n*-type semiconductor with a low band gap of around 2.18 eV. The low band gap makes NiTiO$_3$ suitable for visible light-driven photocatalysis to harvest visible light. Furthermore, the band gap is large enough

* Corresponding Author Email: bac.luonghuu@hust.edu.vn

to provide energetic electrons [9]. Recently, NiTiO$_3$ materials have attracted considerable attention because of their high photocatalytic activity under UV irradiation and remarkably under visible light [10–12]. NiTiO$_3$ ilmenite materials have been known to show interesting magnetic and electric properties [13]. Bulk NiTiO$_3$ exhibited the antiferromagnetism with a Neel temperature of 15-22 K [14]. However, Yuvaraj et al. reported that NiTiO$_3$ nanoparticles exhibited the first order phase transition from antiferromagnetic to ferromagnetic transition where the ferromagnetic interaction between the spins begin from 100 K to 360 K [1]. Recently, Varga et al [15] report the magnetic characteristics of epitaxial NiTiO$_3$ films is polar (and possibly ferroelectric) at room temperature and weakly ferromagnetic below 250K. The ferroelectric properties of this material showed that it has a typical M-E loop [13]. The Ti ions in 3d^0 state of NiTiO$_3$ dominate the ferroelectric polarization. The properties of NiTiO$_3$ ceramics dramatically depended on the fabricated method and doping by a transition metal. Rabigul Tursun et. al. reported that the ferroelectric properties of NiTiO$_3$ synthesized by sol-gel method strongly depended on the ethylene glycol due to the changing the arrangement of cation in the structure which cause the changing in crystal size and crystal distortion [16]. R.Vijayalakshmi investigated the effect of reaction temperature on optical properties of NiTiO$_3$. It showed that optical bandgap decreased when annealing temperature increased from 500°C to 800°C [17]. Currently, there are many reports describing the effect of doping on NiTiO$_3$ materials. For enhancement of magnetic properties, our results show that doping with Fe into NiTiO$_3$ can change the magnetic properties of this material from antiferromagnetic to weak ferromagnetic behavior [18]. However, doping with Co does not have the same behavior as doping with Fe. The magnetic property of Co-doped NiTiO$_3$ still possessed antiferromagnetic characteristics as host material [19]. Fujioka et al. investigated the effect of Co on the structural distortion of NiTiO$_3$ fabricated by solid state method using Raman analysis [20]. Copper doping into NiTiO$_3$ materials showed dramatical change in properties of NiTiO$_3$ which was shown in reports of R. Tursun et al. [21]. The copper doped concentration lower than 5 mol.% caused in change the antiferromagnetic to ferromagnetic behavior of host ceramics while copper concentration

higher than 5 mol% kept no change in magnetic characteristic of host materials. However, there is a lack report of systematic investigation the effect of copper doping on the structural and optical properties of Cu-doped NiTiO$_3$ ceramics, especially tuning in bandgap of this material and the correlation between the structure with optical properties. The present study aimed to investigate the effect of copper dopant in a wide range of concentrations ($0 \leq x \leq 0.1$) on the structural and optical properties of NiTiO$_3$ synthesized by a simple citrate gel method. The structural and optical properties of synthesized materials were investigated by X-ray diffraction (XRD), field emission scanning electron microscopy (FESEM), Raman spectroscopy and UV-vis spectroscopy.

MATERIALS AND METHODS

The NiTiO$_3$ nanoparticles were synthesized by the citrate-gel method using nickel nitrate (Ni(NO$_3$)$_2$.6H$_2$O), copper nitrate (Cu(NO$_3$)$_2$.3H$_2$O) and titanium (IV) isopropoxide (C$_{12}$H$_{28}$O$_4$Ti) as Ni, Cu, Ti sources and citric acid (C$_6$H$_8$O$_7$) as a complexing reagent. Fig. 1 shows the schematic of the citrate gel process for the preparation of the Cu doped NiTiO$_3$ powders. First, the C$_{12}$H$_{28}$O$_4$Ti was dissolved in the C$_6$H$_8$O$_7$ solution at 70 °C. A transparent homogeneous sol was formed after stirring vigorously for 2 h. Then, Ni(NO$_3$)$_2$.6H$_2$O and Cu(NO$_3$)$_2$. 3H$_2$O with equal moles of (Ni+Cu) and Ti was introduced. The resulting solution was continuously stirred for about 4 h to obtain a gel. The gel was oven dried at 120 °C for 24 h to obtain a xerogel. The xerogel was annealed at 800°C in air for 3 h and then milled in an agate mortar to get the powder samples. X-ray diffraction (XRD) pattern of the grilled powders was recorded via Philips X'PertPro X-ray diffractometer using a Ni-filtered Cu Kα radiation (λ = 1.5406 Å) in range of 20°–70°. Field emission scanning electron microscopy images were obtained on JEOL JSM-7600F. The appearance of the chemical element in the final compounds of the sample powder was measured via energy dispersive X-ray spectroscopy (EDX). UV absorbances were determined on a UV–Vis–NIR spectrophotometer (Perkin-Elmer Lambda 1050). The Raman spectra were recorded via micro Raman spectrophotometer (JASCO Raman NRS-3000) using 633 nm excited laser at room temperature.

Photocatalytic measurements were carried out in an aqueous solution of congo red (CR) to evaluate
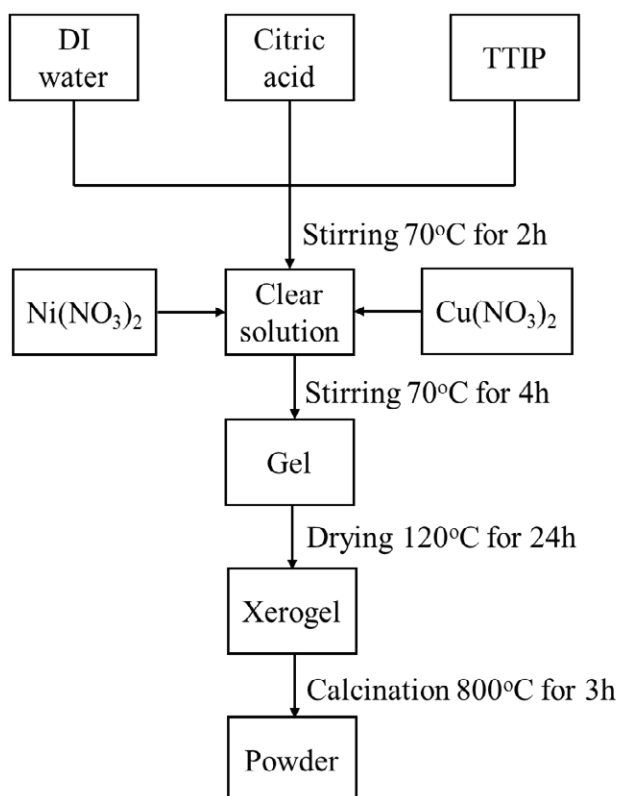
Fig. 1. Schematic diagram describing the synthesis process of Cu doped NiTiO₃ by citrate gel method

effect of Cu dopant on the photocatalytic activity of the fabricated powders. An aqueous solution containing 10^{-4} mol/l of congo red was prepared for photocatalytic degradation. A mixture of 0.1 g of NiTiO₃ powder and 100 mL of CR was stirred for 60 min in the dark to reach an adsorption/desorption equilibrium for CR and oxygen on the surface of NTO powders. After reaching equilibrium adsorption, the suspensions were then illuminated for 18 h using a 50 W phase LED lamp (Model D CP03L/50W, RALACO Co.). The light source was placed at about 15 cm from solution for visible light reaction. At every interval of 2 h, a small amount of 3 mL of the suspension solution was taken out and then separated by centrifugation (4000 rpm, 15 min). The supernatants were analyzed by recording variations of the absorption band maximum in the UV–vis spectra by using a Carry UV/vis spectrophotometer. The quantitative determination of CR was performed by measuring its maximum absorption of UV-Vis at 500 nm. The blank reaction was carried out following the same procedure without adding the catalyst. The photo-degradation was calculated by the following formula:

$$\text{Degradation ration}\,(\%) = \frac{C_o - C}{C_o} \times 100$$

Where Co is the absorbance of CR dye before irradiation and C is the absorbance of CR under diffraction irradiation time intervals.

RESULTS AND DISCUSSION

Fig. 2a shows the XRD patterns for the synthesized powders annealed at 800°C for 3 h. The main diffraction peaks at $2\theta = 24.03°$, 32.99°, 35.55°, 40.76°, 49.34°, 53.90°, 57.35°, 62.35°, and 63.97° of all undoped and doped samples agreed well with standard JCPDS data (no. 83-0198) for the rhombohedral crystal structure R-3 space group. These values indicated the ilmenite structure of synthesized powders. All samples included the diffraction peaks at 2q = 24.03°, 32.99°, 35.55°, 40.76°, 49.34°, 53.90°, 57.35°, 62.35°, and 63.97°, corresponding to the lattice planes of (012), (104), (110), (113), (024), (116), (018), (214), and (300), respectively.

The lattice parameters (a,c) of undoped NiTiO₃
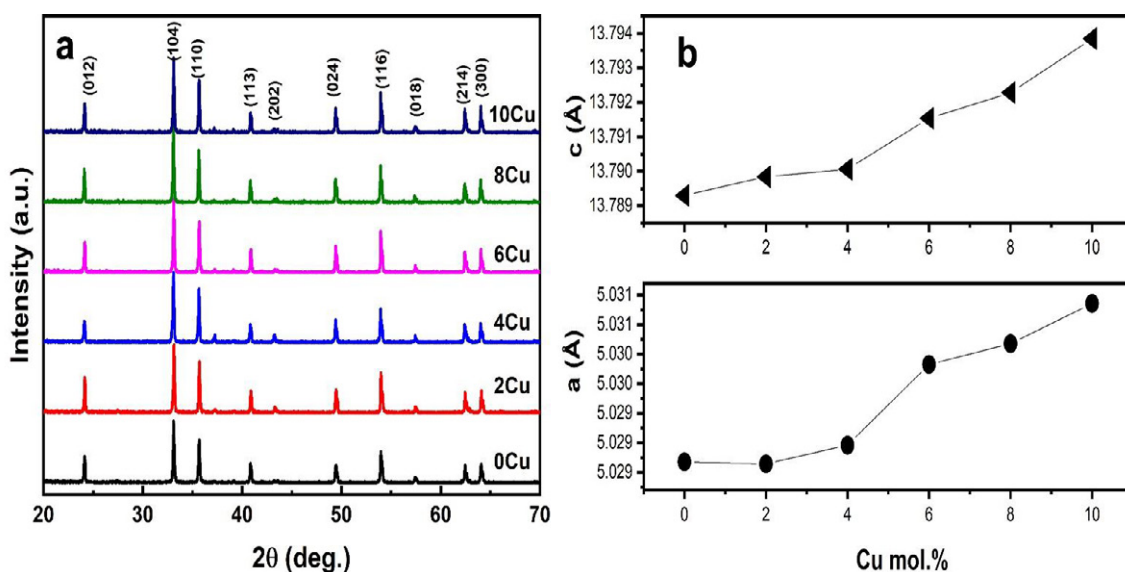
Fig. 2. (**a**) XRD pattern of NiTiO₃ annealed at 800°C in air and (**b**) Unit cell parameters of undoped NiTiO₃ and Cu doped NiTiO₃

and Cu doped NiTiO₃ compound as a function of Cu dopant was shown in Fig. 2b. The results were provided that the trending in distortion lattice parameters of Cu-doped NiTiO₃ compound was nearly linear with the Cu dopant concentration. The expansion of lattice when Cu doped into NiTiO₃ can explain via the difference between the radius of Cu impurities and Ni cations of host lattice materials. Based on Shannon's report, the radius of Cu^{2+} and Ni^{2+} cations in coordination number 6 are 0.73 Å and 0.69 Å, respectively [22]. The radius of the Cu^{2+} is bigger than that of Ni^{2+}, therefore the substitution of Cu^{2+} for Ni^{2+} when doping caused the lattice parameters to expand. The linear dependence of unit cell parameters with the copper content existed because the copper doped into NiTiO₃ can create the formation of a substitutional solid solution in the whole composition range which was investigated. The expansion of unit cell in our work is in agreement with the study of Amandine Guiet et al carried out on Cu doped NiTiO₃ which fabricated by solid state method [23]. The Scherrer crystallite sizes were calculated using all the diffraction peaks appearing in the patterns, according to Scherrer formula $L = k\lambda/\beta\cos\theta$, where λ is the wavelength of the X-ray radiation (Cu Ka = 0.15406 nm), k is the constant taken as 0.89, β is the line width at half maximum height and θ is the diffracting angle. The crystalline grain sizes of NiTiO₃ calculated by Scherrer formula increased from 54 nm to 70

nm when the Cu content increased from 0.0% to 10.0%. These results indicated that the crystallite sizes of the NiTiO₃ materials depended on the Cu content, and the addition of copper promoted the growth of crystalline grains of NiTiO₃.

The results of XRD analysis indicated that the pure NiTiO₃ phase was obtained when the samples were annealed at a temperature of 800°C for 3 h in air. To corroborate the results of XRD analysis, Raman spectroscopy was used to analyze the vibration properties of the fabricated powders. Analysis of Raman scattering spectra can give more evidence of structural changes, crystalline vibrations and distortions of the crystal lattice besides XRD analysis. Fig. 3 shows the Raman scattering of NiTiO₃ samples annealed at temperatures of 800°C. The theoretical calculation indicated that the optical normal modes of vibrations have symmetries represented by $5A_g + 5E_g + 4A_u + 4E_u$, where $5A_g + 5E_g$ are ten active Raman modes, $4A_u + 4E_u$ are inference active modes, and $A_u + E_u$ are two modes inactive in both Raman and inference modes [24–26]. Therefore, ten Raman active modes are expected with each E_g mode being twofold degenerated to $E_g^1 + E_g^2$ along with the eight IR active modes $4A_u + 4E_u$ [26]. The bands located at 608 cm⁻¹ and 704 cm⁻¹ are described to the stretching of Ti–O and bending of O–Ti–O bonds [17]. The band at 227.6 cm⁻¹ can originate from the asymmetric breathing vibration of the oxygen octahedral; the ones at 290.2 and

772
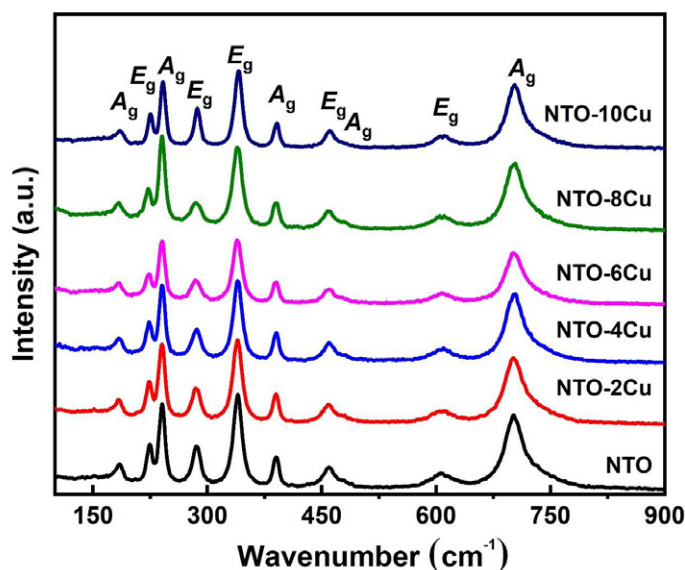
Fig. 3. Raman spectra of NiTiO$_3$ doped with different Cu concentration measured at room temperature

Table 1. The detail parameters of Raman peak of NiTiO$_3$ at around 700 cm^{-1}

Sample	Peak position (cm^{-1})	Peak intensity (a.u.)	FWHM (cm^{-1})
NiTiO$_3$	608.37	703.95	25.91
Ni$_{0.98}$Cu$_{0.02}$TiO$_3$	605.89	703.16	30.55
Ni$_{0.96}$Cu$_{0.04}$TiO$_3$	605.42	703.31	31.62
Ni$_{0.94}$Cu$_{0.06}$TiO$_3$	605.22	703.38	31.49
Ni$_{0.92}$Cu$_{0.08}$TiO$_3$	605.55	703.45	31.56
Ni$_{0.90}$Cu$_{0.10}$TiO$_3$	605.42	703.36	31.72

434.3 cm^{-1} can be attributed by the twist of oxygen octahedral due to the vibrations of the Ni and Ti atoms parallel to the *xy* plane; the E_g modes at 463.4 cm^{-1} and 609.7 cm^{-1} are assigned to the asymmetric breathing and twist of the oxygen octahedral with the cationic vibrations parallel to the *xy* plane [26]. Our result indicated that the Raman spectra were considerably dependent on the copper dopant content. A slight decrease in Raman shift to the lower frequency was observed in Raman spectra of Cu-doped NiTiO$_3$ samples. This shift might be due to bigger ionic radii of Cu^{+2} ion replace at Ni^{+3} site in the lattice of NiTiO$_3$. The substitution of Cu at this site caused the lattice expansion and increased the bond length between cations. The Raman band at 700 cm^{-1} was detailly analyzed and shown in Table 1. The shift of peak position to lower frequency, reduction in the intensity of the peak, and a wider the FWHM value of peak revealed the change in structure of NiTiO$_3$ with presentation of copper dopant (as in Table 1). They indicated the stronger structural disorder, which could be due to the copper substitution in NiTiO$_3$ lattice and caused the local distortion of lattice. By combination between XRD and Raman analysis, we can confirm that the Cu dopant substituted at Ni site in the lattice of NiTiO$_3$ and caused the distortion in lattice crystal of NiTiO$_3$.

Figs. 4a–4g show the surface morphology of undoped and Cu doped NiTiO$_3$ annealed at 800°C. The particles in all samples had irregular shape and were almost similar among all samples. Fig 5a shows the dependence of particle size on the Cu doping content. The results showed that the average particle size tend to increase with increasing of Cu content. The particle size
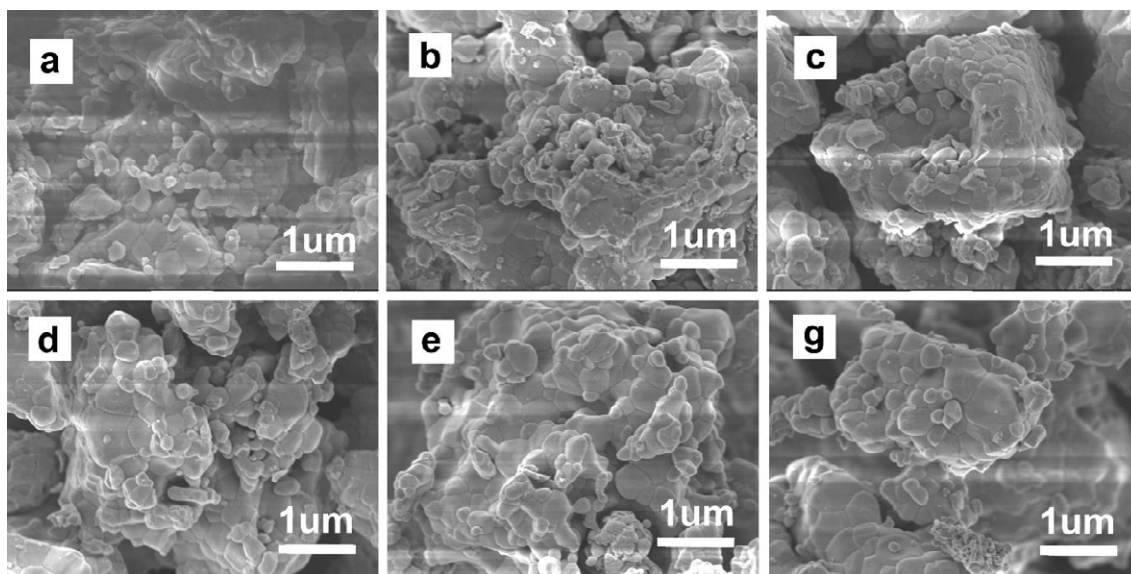
Fig. 4. FE-SEM image of undoped and NiTiO$_3$ doped with different Cu concentration
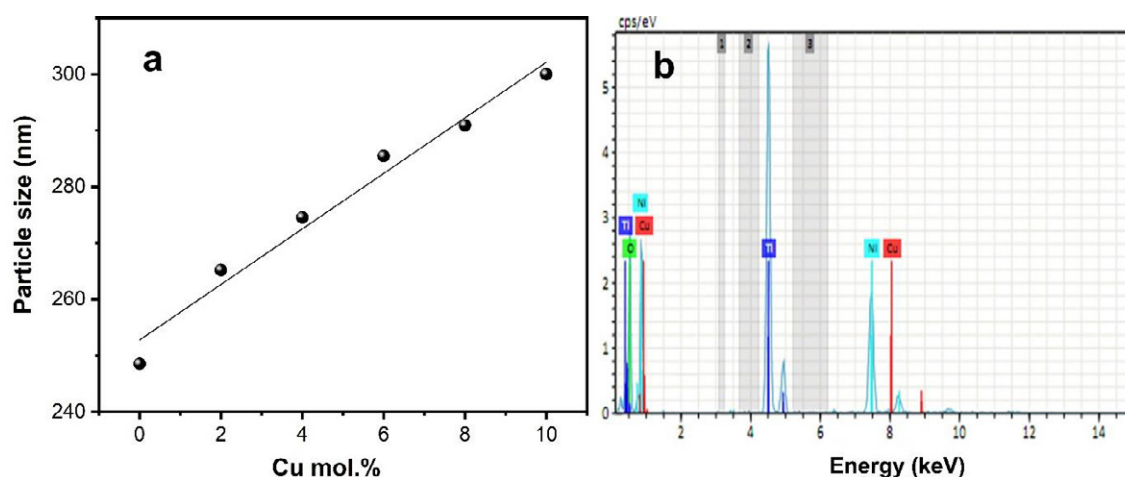
Fig. 5. (**a**) The dependence of particle size on the Cu doped concentration and (b) the EDX of NiTiO$_3$ with 2 mol. % Cu dopant

of undoped sample is about 250 nm. This value increased to about 300 nm of Cu doped 10 mol.% NiTiO$_3$ samples. Copper dopant acted as sintering aid, helping the rising both in crystalline size and particle size of NiTiO$_3$ material. To confirm the copper dopant substitution in the NiTiO3, EDX analysis was used to check the all elements in synthesized samples. The EDX of 2 mol.% Cu-dopant in NiTiO$_3$ was shown in Fig. 5b. It is confirmed that all expected elements appeared in the EDX result which reveals that the Cu doping doped into the NiTiO$_3$ lattice.

Fig. 6a shows the optical absorption spectroscopy of undoped and Cu-doped NiTiO$_3$ annealed at 800°C at room temperature. The absorption band of doped NiTiO$_3$ was similar as undoped NiTiO3 with three wide bands: a sharp band in the blue region around 420 nm ($n3$:$3A_{2g}$ (3F)$\rightarrow$$3T_{1g}$ (3P)), a broad band in the red region between 650–850 nm ($n2$:$3A_{2g}$ (3F)$\rightarrow$$3T_{1g}$ (3F))and a last broad band in the near infra-red between 1100–1400 nm ($n1$:$3A_{2g}$ (3F)$\rightarrow$$3T_{2g}$ (3F)) [27,28]. The absorption spectra of NiTiO$_3$ based materials showed that they absorbed strong in the visible

774
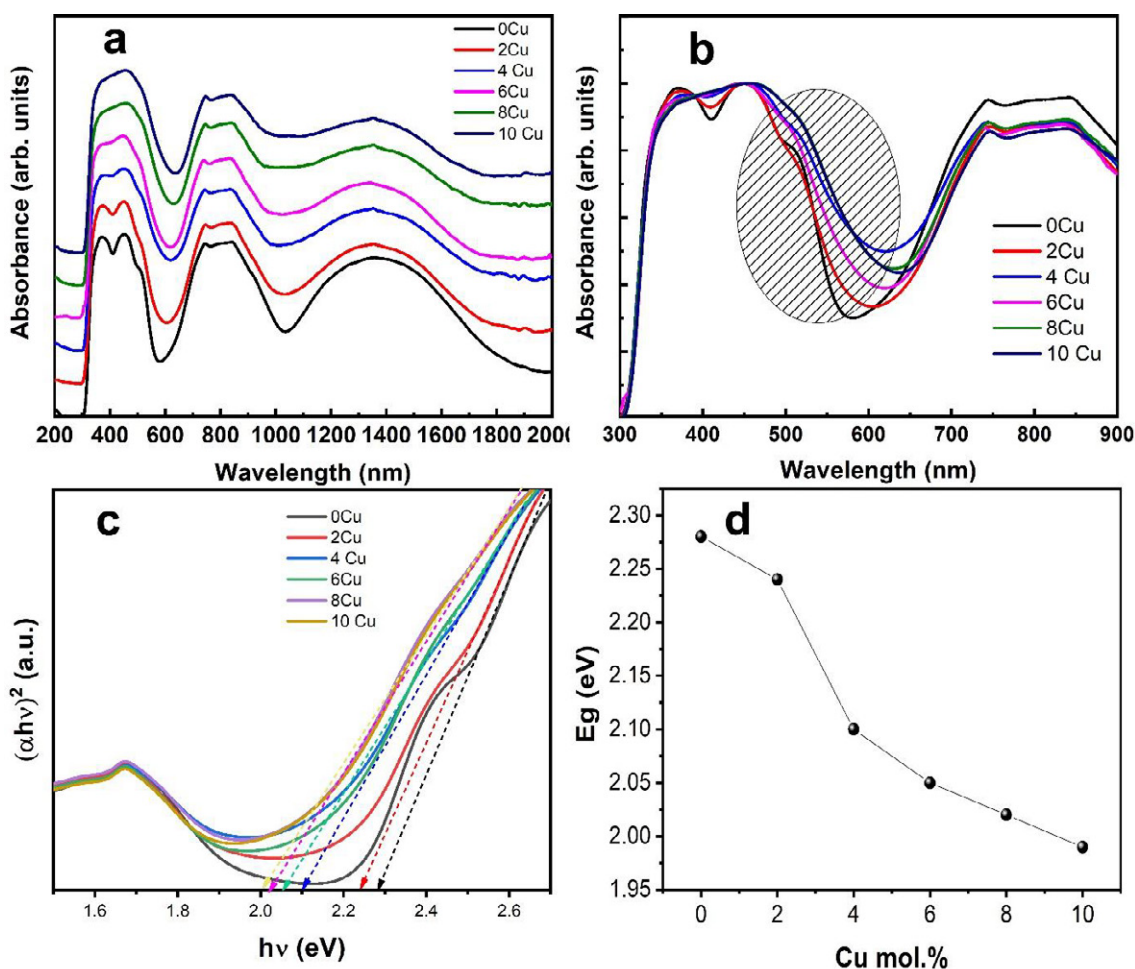
Fig. 6. (**a**) Absorption spectra of undoped and Cu-doped NiTiO$_3$ and (b) the zoom in of absorption spectra in visible region showed the expansion of absorption tail (c) the dependence of (αhν)^2 and (d) the dependence of optical bandgap of undoped and Cu-doped NiTiO$_3$ samples

light which can have feature in photocatalytic characteristic of this material in visible light. The absorption spectra of the fabricated powders all coincided with the spectral features of Ni^{2+} (3d^8 ion) in octahedral coordination. According to Agui and Mizumaki report, three types of electronic transition exist in NiTiO$_3$ material which is between O 2p to Ti 3d, Ni 3d to Ti 3d and Ni 3d to O 2p [29]. The absorption shoulders at around 512 nm may be tentatively assigned to the spin-forbidden transitions 1A_{1g} (1G) + 1T_{2g} (1D) [28]. The first high-intensity absorption band in the near UV (around 365 nm) was associated with the typical charge-transfer transitions O^{2-}–Ti^{4+}. Our results agreed with recently reported optical properties of NiTiO$_3$ materials, where the absorbance peaks resulted from charge transfer from Ni^{2+} to Ti^{4+} caused

by the spin splitting of Ni ions under the crystal field [30]. The positions of those three absorption bands do not change with the Cu substitution in the lattice of NiTiO$_3$, it can be concluded that there is no change in the coordination or in the oxidation state of Ni. Nevertheless, the change in detail of absorption band in the UV region is affected by the copper doping into lattice of NiTiO$_3$. The increased Cu doping concentration resulted in the extension of adsorption tail to longer wavelength such as shown in Fig. 6b. The appearance of tails in doped materials could be related to intrinsic defects and/or surface effects which induced by copper substitution. The change in absorption behavior of copper induced in NiTiO$_3$ resulted in color darkening and is a sign of a reduction optical band gap. The determination of the optical
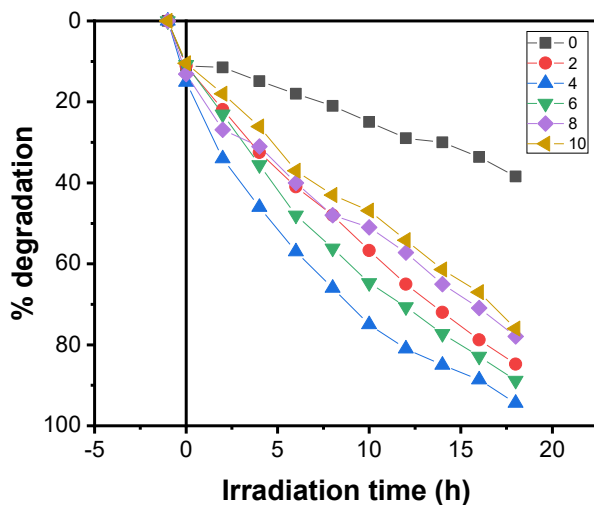
Fig. 7. Photocatalytic degradation of CR on Cu doped NiTiO$_3$ under visible light irradiation.

band gap energy of the ilmenite NiTiO$_3$ material was recently reported both direct and indirect transition. The theoretical prediction for the NiTiO$_3$ materials has indirect transition, whereas the experimental value was estimated from direct transition [31,32]. Optical band gap energy (Eg) of undoped and doped NiTiO$_3$ materials were estimated by Wood and Tauc method [33]. E_g values are associated with the absorbance and photon energy by the following equation $(ahn) \sim (hn-E_g)^n$, where a is the absorbance coefficient, h is the Planck's constant, n is the frequency, E_g is the optical band gap, and n is a constant associated with different types of electronic transition (n = 1/2, 2, 3/2, and 3 for direct allowed, indirect allowed, direct forbidden, and indirect forbidden transitions, respectively). The $(ahn)^2$ as a function of photon energy (hn) were plotted and shown in Fig. 5c and the calculated optical band gaps as a function of Cu dopant content were illustrated in Fig. 5d. For NiTiO$_3$ materials, the largest band gap is expected to relate to the direct electronic transition between the upper edge of O 2p valence band and the lower edge of Ti 3d conduction band. This value is the largest optical band gap for all the samples. The results showed that the value of optical band gap tends to decrease when the concentration of Cu dopant increases. From the plot, it can be seen that the optical band gap was almost linear with Cu content. The undoped NiTiO$_3$ samples annealed at 800 °C exhibited a direct band gap value of 2.31 eV and the bandgap

reduced to 1.99 eV for 10 mol.% Cu doped NiTiO$_3$. The reduction in the optical band gap in Cu-doped Bi$_{0.5}$Na$_{0.5}$TiO$_3$ materials possibly originated from the substitution of Cu cation into the host lattice of NiTiO$_3$ materials. The replacement of Ni cation by transition metals such as Fe in the NiTiO$_3$ materials resulted in the reduction of the optical band gap because the impurities of these transition metal cations formed new local states in the middle of the electronic band structure [18]. Therefore, we suggested that the substitution of Cu in Ni site of NiTiO$_3$ materials was possible to promote the grain size and reduce the optical band gap due to the structural distortion.

Fig. 7 presents the % photodegradation of CR concentration vs. irradiation time for NiTiO$_3$ doping with different Cu concentration under blue LED light irradiation. It is found that the decolorization process of CR proceeds with the increasing irradiation time. The concentration of CR of all sample with undoped NiTiO$_3$ and Cu doped NiTiO$_3$ decreased with increasing of the irradiation time which showed the photocatalytic behavior of based NiTiO$_3$ materials under visible light irradiation. However, the concentration of CR solution increased firstly with low Cu doping concentration and then decreased as the Cu content increased over 4 molar percent. The % degradation reached 95 for 4 % mol. Cu doped NiTiO$_3$, which is much higher than 38 % of undoped NiTiO$_3$. It can be noted that Cu dopant caused the size of NiTiO$_3$ particles increased, thus

it reduced the surface area of particles. However, the CR photodegradation of $NiTiO_3$ doped with Cu element have the better ability in comparison with undoped $NiTiO_3$. It may be the reason that the Cu dopant narrowed the optical bandgap energy. Increasing Cu dopant into $NiTiO_3$ lattice crystal caused the broad adsorption in the visible light region (Fig. 6). A 4% of Cu dopant in $NiTiO_3$ host lattice can acts as an electron scavenger and prevent the combination of electron – hole pairs which could enhance the surface excitation and resulted in the enhancement of photocatalytic efficiency. However, high Cu dopant concentration decreased the photodegradation of $NiTiO_3$. Many experimental results revealed that the photocatalytic activity strongly depended on the dopant concentration [34,35]. The low doping concentration enhanced the photocatalytic efficiency. However, the dopant into the host lattice can act as a mediator of interfacial charge transfer but also act as a recombination center. Therefore, in practice the enhancement will be obtained at the optimal concentration. In this case, the $NiTiO_3$ doped with 4 mol.% has the highest CR photodegradation under visible light irradiation.

CONCLUSIONS

The effect of copper dopant on the structural, optical, and photocatalytic properties of $NiTiO_3$ nanoparticles fabricated by the citrate-gel method was investigated. The undoped and Cu-doped $NiTiO_3$ materials were obtained in pure ilmenite phase. With the increasing Cu content, the increasing crystalline size of $NiTiO_3$ and a noticeable red shift in the UV–Vis absorption are found which caused the reduction of optical band gap from 2.31 eV to 1.99 eV corresponding to the undoped and 10 mol.% Cu dopants, respectively. Copper dopant into $NiTiO_3$ lattice enhanced the photodegradation of congo red under visible light irradiation. Copper dopant has played an important role in the crystalline size and the optical properties of $NiTiO_3$ materials.

ACKNOWLEDGMENTS

CONFLICT OF INTEREST

The authors declare that there is no conflict of interests regarding the publication of this manuscript.

REFERENCES

1. Yuvaraj S, Nithya VD, Fathima KS, Sanjeeviraja C, Selvan GK, Arumugam S, et al. Investigations on the temperature dependent electrical and magnetic properties of NiTiO3 by molten salt synthesis. Materials Research Bulletin. 2013;48(3):1110-6.
2. Jing P, Lan W, Su Q, Yu M, Xie E. Visible-Light Photocatalytic Activity of Novel NiTiO3 Nanowires with Rosary-Like Shape. Science of Advanced Materials. 2014;6(3):434-40.
3. Wang Z, Wang Z, Yang W, Peng R, Lu Y. Carbon-tolerant solid oxide fuel cells using NiTiO3 as an anode internal reforming layer. Journal of Power Sources. 2014;255:404-9.
4. Della Gaspera E, Pujatti M, Guglielmi M, Post ML, Martucci A. Structural evolution and hydrogen sulfide sensing properties of NiTiO3–TiO2 sol–gel thin films containing Au nanoparticles. Materials Science and Engineering: B. 2011;176(9):716-22.
5. Huo K, Li Y, Chen R, Gao B, Peng C, Zhang W, et al. Recyclable Non-Enzymatic Glucose Sensor Based on Ni/NiTiO3/TiO2Nanotube Arrays. ChemPlusChem. 2015;80(3):576-82.
6. Jaye K, Moureen C. Magnetodielectric coupling in the ilmenites MTiO₃ (M = Co, Ni). Physical Review B. 2016;93:104404.
7. Wang J-L, Li Y-Q, Byon Y-J, Mei S-G, Zhang G-L. Synthesis and characterization of NiTiO3 yellow nano pigment with high solar radiation reflection efficiency. Powder Technology. 2013;235:303-6.
8. Lu C-H, Naresh N, Kumar PS, Som S. Microwave-assisted solvothermal synthesis and electrochemical characterizations of ternary perovskite NiTiO3 anode materials for lithium-ion batteries. Ceramics International. 2019;45(15):19517-21.
9. Qu Y, Zhou W, Jiang L, Fu H. Novel heterogeneous CdS nanoparticles/NiTiO3 nanorods with enhanced visible-light-driven photocatalytic activity. RSC Advances. 2013;3(40):18305.
10. Srinivas A, Boey F, Sritharan T, Kim DW, Hong KS, Suryanarayana SV. Study of piezoelectric, magnetic and magnetoelectric measurements on SrBi3Nb2FeO12 ceramic. Ceramics International. 2004;30(7):1431-3.
11. Shu X, He J, Chen D. Visible-Light-Induced Photocatalyst Based on Nickel Titanate Nanoparticles. Industrial & Engineering Chemistry Research. 2008;47(14):4750-3.
12. Sadjadi MS, Mozaffari M, Enhessari M, Zare K. Effects of NiTiO3 nanoparticles supported by mesoporous MCM-41 on photoreduction of methylene blue under UV and visible light irradiation. Superlattices and Microstructures. 2010;47(6):685-94.
13. Acharya T, Choudhary RNP. Structural, Ferroelectric, and Electrical Properties of NiTiO3 Ceramic. Journal of Electronic Materials. 2014;44(1):271-80.
14. Heller GS, Stickler JJ, Kern S, Wold A. Antiferromagnetism in NiTiO3. Journal of Applied Physics. 1963;34(4):1033-4.
15. Varga T, Droubay TC, Bowden ME, Colby RJ, Manandhar S, Shutthanandan V, et al. Coexistence of weak ferromagnetism and polar lattice distortion in epitaxial NiTiO3 thin films of the LiNbO3-type structure. Journal of Vacuum Science & Technology B, Nanotechnology and Microelectronics: Materials, Processing, Measurement, and Phenomena. 2013;31(3):030603.

16. Tursun R, Su Y, Yu Q, Tan J. Room-temperature coexistence of electric and magnetic orders in NiTiO3 and effect of ethylene glycol. Materials Science and Engineering: B. 2018;228:96-102.

17. Ecjhao C. Effect of Reaction Temperature on Size and Optical Properties of NiTiO₃ Nanoparticles. E-Journal of Chemistry. 2012;9(1):282–288.

18. Hung PP, Dung DD, Tuan NH, Trung NN, Bac LH. Iron induced room temperature ferromagnetism in ilmenite NiTiO3 materials. Materials Letters. 2017;209:284-6.

19. Dat TT, Hung PH, Toan DN, Dung DD, Quan CX, Bac LH. Effect of Co doping on properties of ilmenite NiTiO₃. Vietnam Journal of Science and Technology. 2018;56:119–126.

20. Fujioka Y, Frantti J, Puretzky A, King G. Raman Study of the Structural Distortion in the Ni1–xCoxTiO3 Solid Solution. Inorganic Chemistry. 2016;55(18):9436-44.

21. Tursun R, Su YC, Yu QS, Tan J, Hu T, Luo ZB, et al. Effect of doping on the structural, magnetic, and ferroelectric properties of Ni1-xAxTiO3 (A = Mn, Fe, Co, Cu, Zn; x = 0, 0.05, and 0.1). Journal of Alloys and Compounds. 2019;773:288-98.

22. Shannon RD. Revised effective ionic radii and systematic studies of interatomic distances in halides and chalcogenides. Acta Crystallographica Section A. 1976;32(5):751-67.

23. Guiet A, Huan TN, Payen C, Porcher F, Mougel V, Fontecave M, et al. Copper-Substituted NiTiO3 Ilmenite-Type Materials for Oxygen Evolution Reaction. ACS Applied Materials & Interfaces. 2019;11(34):31038-48.

24. Fujioka Y, Frantti J, Puretzky A, King G. Raman Study of the Structural Distortion in the Ni1–xCoxTiO3 Solid Solution. Inorganic Chemistry. 2016;55(18):9436-44.

25. Busca G, Ramis G, Amores JMG, Escribano VS, Piaggio P. FT Raman and FTIR studies of titanias and metatitanate powders. Journal of the Chemical Society, Faraday Transactions. 1994;90(20):3181.

26. Ruiz-Preciado MA, Bulou A, Makowska-Janusik M, Gibaud A, Morales-Acevedo A, Kassiba A. Nickel titanate (NiTiO3) thin films: RF-sputtering synthesis and investigation of related features for photocatalysis. CrystEngComm. 2016;18(18):3229-36.

27. Rossman GR, Shannon RD, Waring RK. Origin of the yellow color of complex nickel oxides. Journal of Solid State Chemistry. 1981;39(3):277-87.

28. Llusar M, García E, García MT, Esteve V, Gargori C, Monrós G. Synthesis and coloring performance of Ni-geikielite (Ni,Mg)TiO3 yellow pigments: Effect of temperature, Ni-doping and synthesis method. Journal of the European Ceramic Society. 2015;35(13):3721-34.

29. Agui A, Mizumaki M. Intermetallic charge transfer and band gap of MTiO3 (M=Mn, Fe, Co, and Ni) studied by O 1s-edge X-ray emission spectroscopy. Journal of Electron Spectroscopy and Related Phenomena. 2011;184(8-10):463-7.

30. Lin Y-J, Chang Y-H, Yang W-D, Tsai B-S. Synthesis and characterization of ilmenite NiTiO3 and CoTiO3 prepared by a modified Pechini method. Journal of Non-Crystalline Solids. 2006;352(8):789-94.

31. Zhang X, Lu B, Li R, Fan C, Liang Z, Han P. Structural, electronic and optical properties of Ilmenite A TiO 3 (A =Fe, Co, Ni). Materials Science in Semiconductor Processing. 2015;39:6-16.

32. Ruiz-Preciado MA, Kassiba A, Gibaud A, Morales-Acevedo A. Comparison of nickel titanate (NiTiO3) powders synthesized by sol–gel and solid state reaction. Materials Science in Semiconductor Processing. 2015;37:171-8.

33. Hill M. Weak absorption tails in amorphous semiconductors. Phys Rev B. 1972;5(8):3144–3151.

34. Krishnakumar V, Boobas S, Jayaprakash J. Effect of Cu doping on TiO₂ nanoparticles and its photocatalytic activity under visible light. Journal of Materials Science: Materials in Electronics. 2016; 27:7438–7447

35. Zhou M, Yu J, Cheng B, Yu H. Preparation and photocatalytic activity of Fe-doped mesoporous titanium dioxide nanocrystalline photocatalysts. Materials Chemistry and Physics. 2005;93(1):159-63.